Advances in Nano Research, *Vol. 17, No. 6 (2024) 547-558*
https://doi.org/10.12989/anr.2024.17.6.547

Nonlinear stability analysis of shear-deformable sandwich meta-composite shell with arc-type auxetic core

Farzad Ebrahimi*[1], Mohammadhossein Goudarzfallahi[2], Ali Alinia Ziazi[2]

[1]*Department of Mechanical Engineering, Faculty of Engineering, Imam Khomeini International University, Qazvin, Iran*
[2]*Mechanical Engineering Department, Science and Research branch, Islamic Azad University, Tehran, Iran*

(*Received March 21, 2019, Revised January 17, 2021, Accepted October 8, 2024*)

Abstract. This paper introduces analytical solutions to study the nonlinear buckling and postbuckling behavior of shear-deformable, arc-type auxetic-core sandwich composite toroidal shell segments (TSSs) with carbon nanotube (CNT)-reinforced face sheets surrounded by Kerr-type foundation and subjected to external pressure. CNTs are incorporated into a polymer matrix with a uniform (UD) or functionally graded (FG) distribution across the shell thickness. Inspired by the traditional concave hexagonal design, the arc-type auxetic core includes curved ribs and allows for a smooth transition between adjacent unit cells, effectively mitigating stress concentrations. The Kerr-type three-parameter elastic foundation is modeled with a central shear layer and two spring layers on both the top and bottom sides. The governing equations for the TSSs are derived using Reddy's third-order shear deformation theory (TSDT), incorporating von Kármán-type geometric nonlinearity. A three-term deflection solution under simply supported boundary conditions is employed, with the Galerkin method used to establish the nonlinear load-deflection relationship. The effectiveness of the current approach is confirmed through comparative analysis with existing literature, demonstrating good agreement with theoretical results. The numerical results examine the effects of geometric parameters of the arc-type auxetic metamaterial structure—specifically the inclined angle of the auxetic core and circular arc radius—along with Kerr-type elastic foundation parameters, CNT distribution, and geometric characteristics on the critical buckling loads and postbuckling paths of sandwich TSSs.

Keywords: arc-type auxetic metamaterial core; buckling and postbuckling; carbon nanotube-reinforced composite; Kerr-type elastic foundation; toroidal shell segment; TSDT

1. Introduction

Auxetic materials are gaining significant attention for research and application in various industries due to their lightweight and exceptional ability to absorb the impact impulses they are subjected to. Compression and shear resistance, energy absorption, low frequency and energy harvesting, and high damping resistance are only some of the mechanical attributes these metamaterials have been shown to improve (Ebrahimi 2024).

Recently, advanced composite materials have been developed by integrating an auxetic core layer into a sandwich-structured composite, significantly enhancing static and dynamic load-carrying capacities. This innovation proves highly beneficial in various applications, including civil engineering, aerospace engineering, and energy absorption systems. Numerous studies have investigated the mechanical performance of plate and shell structures incorporating auxetic cores. Ebrahimi and Dadashi (2023) analyzed the vibration characteristics of a composite cylindrical shell with an auxetic core supported by an elastic foundation and subjected to axial compression and external excitation. Li and Liu (2022) investigated sandwich shells' thermal buckling and free vibration with a tunable auxetic honeycomb core and functionally graded (FG) face sheets. Ebrahimi and Ahari (2024) examined the buckling of composite graphene origami-enabled auxetic metamaterial (GOEAM) nanoplates, which featured magnetostrictive face sheets and were subjected to a temperature gradient. Ghafouri *et al.* (2023) used three-dimensional elasticity theory to study sound transmission loss in a doubly curved sandwich shell with a 3D re-entrant auxetic cellular core. Mahinzare *et al.* (2024) studied the nonlinear vibrations of an intelligent plate with an auxetic core and piezo-electrically-driven multiscale nanocomposite layers. Li *et al.* (2020a) performed a nonlinear dynamic analysis of sandwich plates with a 3D auxetic lattice core. Li *et al.* (2020b) also investigated the response of sandwich cylindrical shells under low-velocity impacts, featuring a 3D double-V auxetic meta-lattice core and FG graphene-reinforced composite (GRC) face sheets. The sound transmission characteristics of sandwich composite doubly-curved shells with an arc-type auxetic cellular core were examined by Wang and Fu (2024), reporting higher sound transmission loss compared to traditional re-entrant types. Fu *et al.* (2024) also investigated the low-velocity impact characteristics of stiffened, porous, doubly-curved sandwich shells with an arc-type auxetic core.

Carbon nanotubes (CNTs) are highly suitable for enhancing composite materials owing to their remarkable mechanical, thermal, and electrical properties. When incorporated as fibers, they can be distributed within a

*Corresponding author, Ph.D.,
E-mail: febrahimy@eng.ikiu.ac.ir

ISSN: 2287-237X (Print), 2287-2388 (Online)

polymeric matrix in either a uniform (UD) or FG manner (Ebrahimi and Dabbagh 2020). Shen (2011a, b) conducted a postbuckling analysis of FG-CNTRC cylindrical shells using Higher-Order Shear Deformation Theory (HSDT), incorporating von Kármán-type kinematic nonlinearity. A perturbation technique was employed to examine the buckling and postbuckling behavior of the cylindrical shells. Duc *et al*. (2020), using Reddy's third-order shear deformation theory (TSDT) and the Galerkin method, presented analytical solutions for the nonlinear buckling behavior of imperfect CNTRC cylindrical panels on elastic foundations. Sofiyev and Kuruoglu (2022) investigated the buckling of conical shells reinforced with CNTs under hydrostatic pressure and axial compression on an elastic foundation. Ebrahimi and Dabbagh (2023) studied the effects of porosity on the static performance of CNT-reinforced meta-nanocomposite structures. Zhao *et al*. (2024) investigated the buckling analysis of CNTRC conical shells using first-order shear deformation theory. Hieu and Van Tung (2021) examined the buckling and postbuckling behavior of CNTRC cylindrical shells exposed to a uniform temperature increase. Shen and Xiang (2013) provided a postbuckling analysis of CNTRC cylindrical shells under axial load and radial pressure in a thermal environment. Chakraborty and Dey (2023) explored the local and global stability of CNTRC sandwich shell panels consisting of CNTRC face sheets and softcore material. Van Quyen *et al*. (2021) investigated the nonlinear vibration of a sandwich composite cylindrical panel with an auxetic honeycomb core and CNTRC face sheets supported by a visco-Pasternak foundation and subjected to blast loading in a thermal environment.

Toroidal shell segments (TSSs) are widely used in various engineering applications, including aeronautical, underwater, and civil structures. By adjusting the radius of curvature, various structural modifications can be achieved. Researchers have extensively studied the static and dynamic stability of TSSs. Using classical shell theory (CST). Stein and McElman (1965) investigated the buckling response of isotropic TSSs under external pressure and axial compression. Using CST, Hutchinson (1967) studied the initial postbuckling behavior of TSSs subject to several loading conditions. Oyesanya (2005) explored the bifurcation of a TSS with initial imperfections subjected to external pressure based on Donnell shell theory. Based on the CST and utilizing Stein and McElman's (1965) approximation, Phuong *et al*. (2021) investigated the nonlinear buckling and post-buckling characteristics of FG-GRC TSSs under radial pressure, surrounded by elastic foundations, and exposed to a thermal environment.

Recently, based on Stein and McElman's (1965) approximation and CST, many studies have focused on improving the buckling and postbuckling behavior of these shells, mainly through the use of advanced nanocomposites combined with auxetic cores (Van Tien *et al*. 2022, Ebrahimi *et al*. 2024a, b, Nguyen *et al*. 2023, Nam *et al*. 2022, Phuong *et al*. 2023, Hoai Nam *et al*. 2024). Van Tien *et al*. (2022) performed a nonlinear analysis of buckling in sandwich TSSs with a honeycomb auxetic core and CNT-reinforced face sheets supported by elastic foundations and subjected to radial pressure. The Galerkin procedure obtained the shell's buckling and postbuckling responses. Ebrahimi *et al*. (2024a) performed a comparative stability analysis of sandwich TSSs using a composite material with a GOREAM core and CNTRC face sheets. Their results showed that the GOREAM core significantly enhanced stability compared to re-entrant auxetic metamaterials. In another study, Ebrahimi *et al*. (2024b) examined the effects of porosity in TSSs with a GOREAM core and CNTRC face sheets, revealing that increased porosity reduces buckling resistance and load-bearing capacity.

Additionally, a few recent studies have focused on the effects of shear deformation on the buckling and post-buckling behavior of TSSs (Dung and Vuong 2017, Hieu and Van Tung 2020a, b, Vuong and Duc 2019, 2020a, b). In their works, Dung and Vuong (2017) studied buckling and postbuckling FGM TSSs under uniform radial pressure, based on TSDT. Hieu and Van Tung (2020a, b), using first-order shear deformation theory, presented an analytical study on the buckling of CNTRC TSSs surrounded by elastic media, considering different loading conditions. Furthermore, in the works of Vuong and Duc (2019, 2020a, b), the buckling and postbuckling characteristics of FG TSSs were studied using the TSDT.

To the authors' knowledge, no prior studies have investigated the buckling and postbuckling behavior of sandwich TSSs with an auxetic-core layer under external pressure using HSDT. Previous works (Van Tien *et al*. 2022, Ebrahimi *et al*. 2024a, b, Nguyen *et al*. 2023, Nam *et al*. 2022, Phuong *et al*. 2023, Hoai Nam *et al*. 2024) focus exclusively on thin shells, disregarding shear deformation effects, essential for improved accuracy in analyzing these structures. Therefore, this study introduces an analytical approach to examine the buckling and postbuckling behavior of shear-deformable sandwich TSSs subjected to external pressure and supported by a Kerr elastic foundation utilizing TSDT. The sandwich structure includes an arc-type auxetic core with a negative Poisson's ratio cellular design and FG-CNT-reinforced face sheets. The arc-type auxetic structure exhibits unique behaviors relative to traditional re-entrant auxetic structures, making it advantageous for lightweight sandwich structures. Based on a re-entrant cellular core, this design includes curved ribs, allowing for a smooth transition between adjacent unit cells and effectively mitigating stress concentrations. Another novel aspect of this study is using a Kerr foundation model to simulate the interaction between the TSSs and the foundation, which has not been explored in existing literature. Moreover, this study will clearly show the difference between critical loads found by TSDT and those found by the CST. This work provides an extensive reference and valuable insights into designing and utilizing sandwich shell structures with auxetic cores, specifically to enhance structural stability.

2. Geometrical and material description

2.1 Geometrical model

Consider TSSs with concave (exhibiting negative Gaussian curvature) and convex (showing positive Gaussian

curvature) configurations, as illustrated in Fig. 1a, where a and R represent the longitudinal and circumferential radii, respectively; h is TSS's total thickness, and L indicates the longitudinal length of the shell. A coordinate system (x,y,z) is defined with origin O positioned at the mid-surface and the end of the shell. The x and y axes represent the longitudinal and circumferential directions, with the z-axis aligning in the radial direction and pointing inward, as illustrated in Fig. 1. The sandwich structure comprises an auxetic core with a thickness of h_2 and two face sheets reinforced with CNTs, each with a thickness of h_1. The sandwich TSSs are surrounded by Kerr's foundation, comprising two springs linked by a shear layer (Fig. 2b).

2.2 Material description

2.2.1 Effective mechanical characteristics of the arc-type auxetic core

This study considers an arc-type auxetic structure as the core layer of the sandwich TSS. By integrating curved ribs into the traditional re-entrant honeycomb design, the core is categorized as an arc-type auxetic structure with a negative Poisson's ratio. This approach minimizes stress concentration within the auxetic structure, facilitating a smoother transition between adjacent unit cells. A schematic representation of the sandwich shell featuring the arc-type auxetic core layer and CNT-reinforced face sheets is shown in Fig. 2.

The equivalent elastic properties of the arc-type auxetic core can be expressed as (Wang and Fu 2024, Fu *et al.* 2024):

$$
\begin{aligned}
E_1^c &= \frac{a_1 \cdot E_c \cdot d_1^3}{12 b_1 r_c^3 (4\theta\cos^2\theta - 3\sin 2\theta + 2\theta)} \\
E_2^c &= \frac{b_1 \cdot E_c \cdot d_1^3}{3 a_1 r_c^3 [4\theta\sin^2\theta + 3\sin 2\theta + 2\theta - 8\sin\theta]} \\
\nu_{12}^c &= \frac{a_1 (3\cos 2\theta/4 + \theta\sin 2\theta/2 - \cos\theta + 1/4)}{b_1 (2\theta\cos^2\theta - 3\sin 2\theta/2 + \theta)} \\
\nu_{21}^c &= \frac{-4\, a_1 (\sin^2\theta + 2\cos\theta(1-\cos\theta) - \theta\sin 2\theta)}{a_1 (2\theta + 3\sin 2\theta + 4\theta\sin^2\theta - 8\sin\theta)} \\
G_{13}^c = G_{23}^c &= \frac{E_c \cdot d_1^3}{8 r_c^3 \begin{bmatrix} \theta\sin^2(\theta) + 2\sin(\theta)(\cos(\theta) - 1) \\ +\theta/2 - \sin(2\theta)/4 \end{bmatrix}} \\
G_{12}^c &= \frac{\begin{matrix} a_1 E_c d_1^3 (2\theta\cos^2\theta - 3sin2\theta/2 + \theta)/ \\ 12 r_c^3 (4\cos^2\theta - 5\sin(2\theta) + 2\theta \end{matrix}}{\begin{matrix} b_1 (2\theta\cos^2\theta - 3\sin 2\theta/2 + \theta) \\ +2 a_1 (3\cos 2\theta/4 - \cos\theta + \theta\sin 2\theta/2 + 1/4) \end{matrix}} \\
\rho^c &= \rho \frac{S_1}{S_2}
\end{aligned}
\tag{1}
$$

where E_c represents the Young's modulus of the original material. Furthermore, the key geometric parameters a_1 and b_1 are expressed as

$$
\begin{aligned}
a_1 &= 2(2r_c + d_1) \times \sin\theta,\ b_1 = 2(2r_c + d_1) \times \cos\theta \\
S_1 &= 80\pi(2r_c d_1 + d_1^3)/360^\circ + 4 d_1 r_c,\ S_2 = 2 a_1 b_1
\end{aligned}
\tag{2}
$$

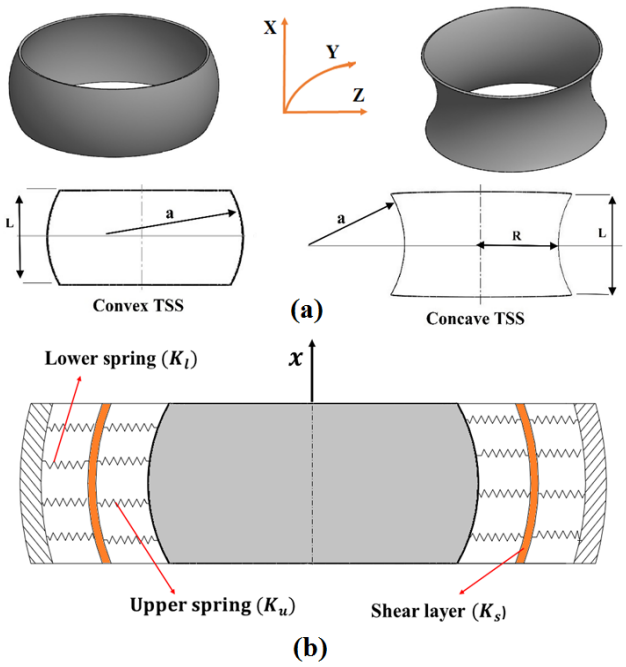

Fig. 1 Configuration of convex and concave TSSs surrounded by Kerr-type elastic foundation

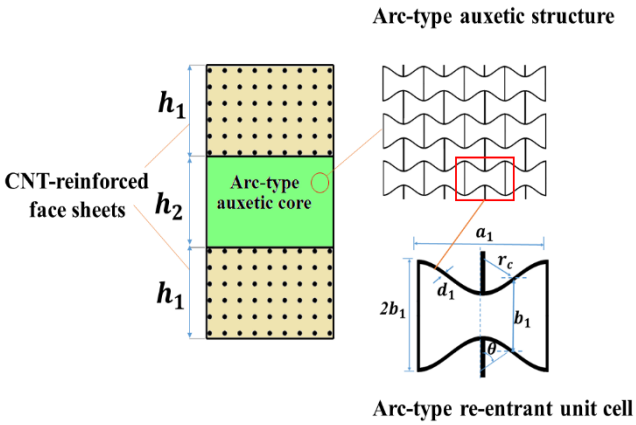

Fig. 2 Configuration of sandwich composite structure with arc-type auxetic core layer and CNT-reinforced face sheets

2.2.2 Effective mechanical properties of CNT-reinforced face sheets

The two face sheets of the sandwich TSS structure are reinforced with CNTs, which have uniform distribution (UD) and FG distributions through the thickness, as shown in Fig. 2. The CNTs are embedded in a poly (methyl methacrylate) (PMMA) matrix, reinforced in either the longitudinal or circumferential directions of the shells. Fig. 2 presents a schematic representation of the sandwich shell, featuring an arc-type auxetic core layer and CNT-reinforced face sheets. This study considers three types of CNT distributions for the face sheets: uniform distribution (UD), FG-X, and FG-O. Furthermore, this research examines the direction of CNT reinforcement from both circumferential and longitudinal perspectives.

The CNT volume fractions in the face sheets are defined as Shen (2011a, b):

$$V_{CNT} = \bar{V}_{CNT}\ (\text{UD})$$
$$V_{CNT} = \left(\frac{4|z|}{h_1}\right)\bar{V}_{CNT}\ (\text{FG}-\text{X})$$
$$V_{CNT} = \left(2-\frac{4|z|}{h_1}\right)\bar{V}_{CNT}\ (\text{FG}-\text{O}) \quad (3)$$

in which $\bar{V}_{CNT}$ is the volume fraction of the CNT. The extended rule of mixture is used for determining the elastic constants of orthotropic material in the CNT-reinforced face sheets, as presented by Shen (2011a, b):

$$E_{11}^{CNTRC} = V_{ma}E_{ma} + \eta_1 V_{CNT}E_{11}^{CNT},$$
$$E_{22}^{CNTRC} = \eta_2 / \left(\frac{V_{CNT}}{E_{22}^{CNT}} + \frac{V_{ma}}{E_{ma}}\right)$$
$$G_{12}^{CNTRC} = \eta_3 / \left(\frac{V_{CNT}}{G_{12}^{CNT}} + \frac{V_{ma}}{G_{ma}}\right), \quad (4)$$
$$\nu_{12}^{CNTRC} = V_{ma}\nu_{ma} + V_{CNT}\nu_{12}^{CNT}$$

in which E_{11}^{CNT}, E_{22}^{CNT}, and G_{12}^{CNT} represent the elastic moduli for the CNTs, while E_{ma} and G_{ma} denote the elastic moduli of the matrix material. Additionally, η_j(j = 1, 2, 3) signifies the performance parameter for the CNTs, and V_{CNT} and V_{ma} are the volume fractions of the CNTs and the matrix, respectively, satisfying the relationship $V_{\text{CNT}} + V_{ma} = 1$. Furthermore, Poisson's ratios for the CNTs and matrix materials are referred to as ν_{12}^{CNT} and ν_{ma}, respectively.

3. Fundamental equations

In the present approach, the TSDT, developed by Reddy and Liu (1987) and considering von Kármán nonlinearity, is applied to establish the governing equations for the nonlinear buckling and postbuckling of auxetic-core sandwich TSSs subjected to uniform external pressure and surrounded by a Kerr-type elastic foundation.

Based on the TSDT, the displacement components at a distance z from the mid-surface are expressed as (Reddy and Liu 1987, Reddy 2003):

$$\begin{pmatrix}\bar{u}\\ \bar{v}\\ \bar{w}\end{pmatrix} = \begin{pmatrix} u + z\phi_x - \frac{4}{3h^2}z^3(\phi_x + \frac{\partial w_0}{\partial x}) \\ v + z\phi_y - \frac{4}{3h^2}z^3(\phi_y + \frac{\partial w_0}{\partial y}) \\ w \end{pmatrix} \quad (5)$$

Here, u, v and w represent the mid-surface displacement components, while ϕ_x and ϕ_y denote the rotations of the normal to the mid-surface with respect to the *y* and *x* axes, respectively.

The strain components at a distance *z* from the mid-surface, incorporating von Kármán nonlinear terms, are given by (Reddy and Liu 1987, Reddy 2003):

$$\begin{pmatrix}\varepsilon_x\\ \varepsilon_y\\ \gamma_{xy}\end{pmatrix} = \begin{pmatrix}\varepsilon_x^0\\ \varepsilon_y^0\\ \gamma_{xy}^0\end{pmatrix} + z\begin{pmatrix}k_x^{(1)}\\ k_y^{(1)}\\ k_{xy}^{(1)}\end{pmatrix} + z^3\begin{pmatrix}k_x^{(3)}\\ k_y^{(3)}\\ k_{xy}^{(3)}\end{pmatrix} \quad (6)$$

$$\begin{pmatrix}\gamma_{xz}\\ \gamma_{yz}\end{pmatrix} = \begin{pmatrix}\gamma_{xz}^0\\ \gamma_{yz}^0\end{pmatrix} + z^2\begin{pmatrix}k_{xz}^{(2)}\\ k_{yz}^{(2)}\end{pmatrix}$$

The strain components at the mid-surface of the shell are expressed in terms of the displacements u, v and w as (Stein and McElman 1965, Reddy 2003):

$$\begin{pmatrix}\varepsilon_x^0\\ \varepsilon_y^0\\ \gamma_{xy}^0\end{pmatrix} = \begin{pmatrix}u_{,x} - w/a + w_{,x}^2/2\\ v_{,y} - w/R + w_{,y}^2/2\\ u_{,y} + v_{,x} + w_{,x}w_{,y}\end{pmatrix}, \quad (7)$$
$$\begin{pmatrix}\gamma_{xz}^0\\ \gamma_{yz}^0\end{pmatrix} = \begin{pmatrix}\phi_x + w_{,x}\\ \phi_y + w_{,y}\end{pmatrix}$$

Furthermore:

$$\begin{pmatrix}k_x^{(1)}\\ k_y^{(1)}\\ k_{xy}^{(1)}\end{pmatrix} = \begin{pmatrix}\phi_{x,x}\\ \phi_{y,y}\\ \phi_{x,y} + \phi_{y,x}\end{pmatrix},$$
$$\begin{pmatrix}k_x^{(3)}\\ k_y^{(3)}\\ k_{xy}^{(3)}\end{pmatrix} = -c\begin{pmatrix}\phi_{x,x} + w_{,xx}\\ \phi_{y,y} + w_{,yy}\\ \phi_{x,y} + \phi_{y,x} + 2w_{,xy}\end{pmatrix} \quad (8)$$
$$\begin{pmatrix}k_{xz}^{(2)}\\ k_{yz}^{(2)}\end{pmatrix} = -3c\begin{pmatrix}\phi_x + w_{,x}\\ \phi_y + w_{,y}\end{pmatrix} \quad c = 4/3h^2$$

By applying Hooke's law, the constitutive stress-strain equations for the TSSs are given by

$$\begin{pmatrix}\sigma_x\\ \sigma_y\\ \sigma_{yz}\\ \sigma_{xz}\\ \sigma_{xy}\end{pmatrix} = \begin{bmatrix}Q_{11} & Q_{12} & 0 & 0 & 0\\ Q_{12} & Q_{22} & 0 & 0 & 0\\ 0 & 0 & Q_{55} & 0 & 0\\ 0 & 0 & 0 & Q_{44} & 0\\ 0 & 0 & 0 & 0 & Q_{66}\end{bmatrix} \quad (9)$$

where

$$Q_{11} = \frac{E_{11}}{1-\nu_{12}\nu_{21}}, \qquad Q_{12} = \frac{\nu_{21}E_{11}}{1-\nu_{12}\nu_{21}},$$
$$Q_{22} = \frac{E_{22}}{1-\nu_{12}\nu_{21}}, \qquad Q_{44} = G_{23}, \quad (10)$$
$$Q_{55} = G_{13}, \quad Q_{66} = G_{12}$$

The force and moment resultants are represented as

$$(N_i, M_i, P_i) = \int_{-h/2}^{h/2}\sigma_i\,(1, z, z^3)dz, \quad i = x, y, xy$$
$$(Q_j, R_j) = \int_{-h/2}^{h/2}\sigma_{iz}\,(1, z^2)dz, \quad i = x, y \quad (11)$$

Substituting Eq. (6) into Eq. (9), followed by incorporating the results into Eq. (11), provides the constitutive relations as

$$N_x = A_{11}\epsilon_x^0 + A_{12}\epsilon_y^0 + A_{13}k_x + A_{14}k_y + A_{15}k_x^3 + A_{16}k_y^3 - A_{17}\Phi_{,y}$$

$$N_y = A_{12}\epsilon_x^0 + A_{22}\epsilon_y^0 + A_{23}k_x + A_{24}k_y + A_{25}k_x^3 + A_{26}k_y^3 - A_{27}\Phi_{,y} \quad (12)$$

$$N_{xy} = A_{31}\gamma_{xy}^0 + A_{32}k_{xy} + A_{33}k_{xy}^3$$

$$M_x = A_{13}\epsilon_x^0 + A_{14}\epsilon_y^0 + A_{43}k_x + A_{44}k_y + A_{45}k_x^3 + A_{46}k_y^3 - A_{17}\Phi_{,y}$$

$$M_y = A_{14}\epsilon_x^0 + A_{24}\epsilon_y^0 + A_{44}k_x + A_{54}k_y + A_{46}k_x^3 + A_{56}k_y^3 - A_{27}\Phi_{,y}$$

$$M_{xy} = A_{32}\gamma_{xy}^0 + A_{62}k_{xy} + A_{63}k_{xy}^3$$

$$P_x = A_{71}\epsilon_x^0 + A_{16}\epsilon_y^0 + B_{73}k_x + A_{46}k_y + A_{75}k_x^3 + A_{76}k_y^3 - A_{17}\Phi_{,x}$$

$$P_y = A_{16}\epsilon_x^0 + A_{82}\epsilon_y^0 + A_{46}k_x + A_{84}k_y + A_{76}k_x^3 + A_{86}k_y^3 - A_{27}\Phi_{,y}$$

$$P_{xy} = A_{33}\gamma_{xy}^0 + A_{63}k_{xy} + A_{93}k_{xy}^3 Q_x = A_{94}\gamma_{xy}^0 + A_{95}k_{xz}^2$$

$$Q_y = A_{96}\gamma_{xy}^0 + A_{97}k_{yz}^2$$

$$K_x = A_{98}\gamma_{xz}^0 + A_{99}k_{xz}^2$$

$$K_y = A_{100}\gamma_{xy}^0 + A_{101}k_{yz}^2$$

Here, the coefficients A_{ij} are determined, as explained by Duc *et al*. (2020).

Based on TSDT, the nonlinear equilibrium equations for sandwich TSSs with an auxetic core and CNT-reinforced face sheets surrounded by a Kerr-type foundation are given as follows (Reddy 2003):

$$N_{x,x} + N_{xy,y} = 0 \\ N_{xy,x} + N_{y,y} = 0 \tag{13}$$

$$Q_{x,x} + Q_{y,y} - 3c\left(R_{x,x} + R_{y,y}\right) + c\left(P_{x,xx} + 2P_{xy,xy} + P_{y,yy}\right) + \frac{N_x}{a} + \frac{N_y}{R} + p_0 + N_x w_{xx} + 2N_{xy}w_{xy} + N_y w_{yy} - k_1 w + k_2(w_{xx} + w_{yy}) = 0 \tag{14}$$

$$M_{x,x} + M_{xy,y} - Q_x + 3cR_x - c\left(P_{x,x} + P_{xy,y}\right) = 0 \tag{15}$$

$$M_{y,y} + M_{xy,x} - Q_y + 3cR_y - c\left(P_{y,y} + P_{xy,x}\right) = 0 \tag{16}$$

Here, the symbol p_0 represents the uniform external pressure. Additionally, $K_1 = K_l K_u/(K_l + K_u)$ and $K_2 = K_s K_u/(K_l + K_u)$ are the elastic foundation parameters, where. K_s is the shear layer stiffness, and K_s and K_l are the stiffness of the top and bottom linear elastic layers, respectively.

Next, the Airy stress function $\varsigma(x, y)$ is introduced as:

$$\varsigma_{,yy} = N_x,\ \varsigma_{,xx} = N_y,\ \varsigma_{,xy} = -N_{xy} \tag{17}$$

Accordingly, one can express the strain components in terms of the stress function ς and the deflection function w as follows:

$$\epsilon_x^0 = \frac{B_{22}}{\Delta}\varsigma_{,yy} - \frac{B_{12}}{\Delta}\varsigma_{,xx} - \frac{B_{13}B_{22} - B_{14}B_{12}}{\Delta}k_x^1 - \frac{B_{14}B_{22} - B_{24}B_{12}}{\Delta}k_y^1 - \frac{B_{15}B_{22} - B_{16}B_{12}}{\Delta}k_x^3 - \frac{B_{16}B_{22} - B_{26}B_{12}}{\Delta}k_y^3$$

$$\epsilon_y^0 = \frac{B_{11}}{\Delta}\varsigma_{,xx} - \frac{B_{12}}{\Delta}\varsigma_{,yy} - \frac{B_{11}B_{14} - B_{13}B_{12}}{\Delta}k_x^1 - \frac{B_{11}B_{24} - B_{14}B_{12}}{\Delta}k_y^1 - \frac{B_{11}B_{16} - B_{15}B_{12}}{\Delta}k_x^3 - \frac{B_{11}B_{26} - B_{16}B_{12}}{\Delta}k_y^3$$

$$\gamma_{xy}^0 = -\frac{1}{B_{31}}\varsigma_{,xy} - \frac{B_{32}}{B_{31}}k_{xy}^1 - \frac{B_{33}}{B_{31}}k_{xy}^3 \tag{18}$$

In which $\Delta = B_{11}B_{22} - B_{12}^2$

From Eq. (7), the compatibility equation for sandwich-structured TSSs is written as:

$$\varepsilon_{x,yy}^0 + \varepsilon_{y,xx}^0 - \gamma_{xy,xy}^0 + \frac{1}{R}w_{,xx} + \frac{1}{a}w_{,yy} - w_{,xy}^2 + w_{,xx}w_{,yy} = 0 \tag{19}$$

Upon substituting Eq. (18) into Eq. (12) and applying the resulting expressions in Eqs. (13)-(16), the equilibrium equations are expressed as follows:

$$H_{11}(\phi_x) + H_{12}(\phi_y) + H_{13}(w) + H_{14}(\varsigma) + P(w, \varsigma) + p_0 = 0 \tag{20}$$

$$H_{21}(\phi_x) + H_{22}(\phi_y) + H_{23}(w) + L_{24}(\varsigma) = 0 \tag{21}$$

$$H_{31}(\phi_x) + H_{32}(\phi_y) + H_{33}(w) + L_{34}(\varsigma) = 0 \tag{22}$$

where

$$H_{11}(\varphi_x) = D_{11}\varphi_{x,x} + D_{12}\varphi_{x,xxx} + D_{13}\varphi_{y,xyy},$$
$$H_{12}(\varphi_y) = D_{21}\varphi_{y,y} + D_{22}\varphi_{y,xxy} + D_{23}\varphi_{y,yyy}$$
$$H_{13}(w) = D_{31}w_{,xx} + D_{32}w_{,yy} + D_{33}w_{,xxxx} + D_{34}w_{,yyyy} + D_{35}w_{,xxyy} - k_1 w + k_2(w_{,xx} + w_{,yy})$$
$$H_{14}(\varsigma) = D_{11}^*\varsigma_{,xxxx} + D_{12}^*\varsigma_{,xxyy} + D_{13}^*\varsigma_{,yyyy} + \frac{\varsigma_{,xx}}{R} + \frac{\varsigma_{,yy}}{a},$$
$$H_{22}(\varphi_y) = D_{51}\varphi_{y,xy}$$
$$P(w, \varsigma) = \varsigma_{,yy}w_{,xx} - 2\varsigma_{,xy}w_{,xy} + \varsigma_{,yy}w_{,yy},$$
$$H_{21}(\varphi_x) = D_{41}\varphi_x + D_{42}\varphi_{x,xx} + D_{43}\varphi_{x,yy}$$
$$H_{23}(w) = D_{61}w_{,x} + D_{62}w_{,xxx} + D_{63}w_{,xyy},$$
$$H_{24}(\varsigma) = D_{21}^*\varsigma_{,xyy} + D_{22}^*\varsigma_{,xxx}$$
$$H_{31}(\varphi_x) = D_{71}\varphi_{x,xy},$$
$$H_{32}(\varphi_y) = D_{81}\varphi_{y,yy} + D_{82}\varphi_{y,xx} + D_{83}\varphi_y$$
$$H_{33}(w) = D_{91}w_{,y} + D_{92}w_{,xxy} + D_{93}w_{,yyy},$$
$$H_{34}(\varsigma) = D_{31}^*\varsigma_{,yyy} + D_{32}^*\varsigma_{,yxx} \tag{23}$$

The expressions for D_{ij} and D_{ij}^* are obtained as described by Dung and Vuong (2017).

By inserting Eq. (18) into Eq. (19), we obtain the compatibility equation for the sandwich TSSs with an auxetic core and CNTRC face sheets as

$$
\begin{aligned}
&I_1\varsigma_{,yyyy} + I_2\varsigma_{,xxxx} + I_3\varsigma_{,xxyy} + I_4\varsigma_{y,yyy} \\
&+I_5\phi_{x,xyy} + I_6\varphi_{x,xxx} + I_7\varphi_{y,xxy} + I_8 w_{,xxxx} \\
&+I_9 w_{,yyyy} + I_{10} w_{,xxyy} \\
&= w_{,xy}^2 - w_{,xx}w_{,yy} - \frac{w_{,xx}}{R} - \frac{w_{,yy}}{a}
\end{aligned} \tag{24}
$$

where

$$
\begin{aligned}
&I_1 = \frac{A_{22}}{\Delta}, \quad I_2 = \frac{A_{11}}{\Delta}, \quad I_3 = \left(\frac{1}{A_{31}} - 2\frac{A_{12}}{\Delta}\right) \\
&I_4 = \left(c_1\frac{A_{16}A_{22} - A_{26}A_{12}}{\Delta} - \frac{A_{14}A_{22} - A_{24}A_{12}}{\Delta}\right) \\
&I_5 = \left(c_1\frac{A_{15}A_{22} - A_{16}A_{12}}{\Delta} - \frac{A_{13}A_{22} - A_{14}A_{12}}{\Delta} \right. \\
&\qquad \left. - c_1\frac{A_{33}}{A_{31}} + \frac{A_{32}}{A_{31}}\right) \\
&I_6 = \left(c_1\frac{A_{11}A_{16} - A_{15}A_{12}}{\Delta} - \frac{A_{11}A_{14} - A_{13}A_{12}}{\Delta}\right) \\
&I_7 = \left(c_1\frac{A_{11}A_{26} - A_{16}A_{12}}{\Delta} - \frac{A_{11}A_{24} - A_{14}A_{12}}{\Delta} \right. \\
&\qquad \left. - c_1\frac{A_{33}}{A_{31}} + \frac{A_{32}}{A_{31}}\right) \\
&I_8 = c_1\frac{A_{11}A_{16} - A_{15}A_{12}}{\Delta}, \quad I_9 = c_1\frac{A_{16}A_{22} - A_{26}A_{12}}{\Delta} \\
&I_{10} = \left(c_1\frac{A_{11}A_{26} - A_{16}A_{12}}{\Delta} + c_1\frac{A_{15}A_{22} - A_{16}A_{12}}{\Delta} \right. \\
&\qquad \left. - 2c_1\frac{A_{33}}{A_{31}}\right) \\
&\Delta = A_{11}A_{22} - A_{12}^2
\end{aligned} \tag{25}
$$

Eqs. (20)-(22) and Eq. (24) serve as the governing equations for analyzing the buckling and postbuckling of sandwich TSSs with an arc-type auxetic core and FG-CNT-reinforced face sheets surrounded by a Kerr-type foundation.

4. Analytical solution

This study considers the auxetic-core sandwich TSSs to be simply supported at both ends, freely movable in the axial direction, and subjected to an external uniform pressure p_0. The boundary conditions are specified as

$$
\begin{aligned}
&w = 0, \quad M_x = 0, \quad N_x = 0, \quad N_{xy} = 0, \\
&\phi_y = 0 \quad \text{at} \quad x = 0;\ x = L
\end{aligned} \tag{26}
$$

The deflection of the shell, $w(x,y)$, which satisfies the boundary conditions (Eq. 26) in an average sense, can be approximated by a three-term expression as follows:

$$
w = W_0 + W_1 sin\frac{m\pi x}{L} sin\frac{ny}{R} + W_2 sin^2\frac{m\pi x}{L} \tag{27}
$$

Here, m and n denote the number of half-waves in the axial and circumferential directions, W_0 is the pre-buckling deflection amplitude, and W_1 and W_2 are the linear and nonlinear postbuckling deflection amplitudes.

Inserting Eq. (27) into the compatibility Eq. (24) and applying the boundary conditions (Eq. 26), the solution of stress function $\varsigma(x,y)$ may be found as

$$
\begin{aligned}
\varsigma &= \varsigma_1\cos\left(\frac{2m\pi x}{L}\right) + \varsigma_2\cos\left(\frac{2ny}{R}\right) \\
&+\varsigma_3\sin\left(\frac{3m\pi x}{L}\right)\sin\left(\frac{ny}{R}\right) + \varsigma_4\sin\left(\frac{3m\pi x}{L}\right)\sin\left(\frac{ny}{R}\right) \\
&-\frac{1}{2}\sigma_{0y}hx^2
\end{aligned} \tag{28}
$$

where σ_{0y} denotes the negative average circumferential stress.

On the other hand, the obtained solution for the stress function should satisfy both Eq. (21) and Eq. (22). This requirement can be fulfilled if the functions ϕ_x and ϕ_y are expressed as

$$
\begin{aligned}
\phi_x(x,y) &= C_1\cos\left(\frac{m\pi x}{L}\right)\sin\left(\frac{ny}{R}\right) + C_2\sin\left(\frac{2m\pi x}{L}\right) \\
&+C_3\cos\left(\frac{3m\pi x}{L}\right)\sin\left(\frac{ny}{R}\right) \\
\phi_y(x,y) &= C_4\cos\left(\frac{ny}{R}\right)\sin\left(\frac{m\pi x}{L}\right) \\
&+C_5\cos\left(\frac{ny}{R}\right)\sin\left(\frac{3m\pi x}{L}\right) + C_6\sin\left(\frac{2ny}{R}\right)
\end{aligned} \tag{29}
$$

Consequently, upon substituting Eqs. (28)-(29) into Eqs. (21)-(22) and solving the resulting equations, the parameters $\varsigma_i(i = 1,4)$ and $C_i(i = 1,6)$ can be found as:

$$
\begin{aligned}
&\varsigma_1 = -a_{15}W_2 + a_{16}W_1^2, \ \varsigma_2 = a_{12}W_1^2, \\
&\varsigma_3 = -\frac{d_{26}W_1 + (d_{15}d_{18}d_{22} - d_{15}d_{16}d_{20})W_1W_2}{d_{24}}, \\
&\varsigma_4 = b_{23}W_1W_2, \\
&C_1 = -\frac{d_{25}W_1 + (d_{15}d_{17}d_{20} + d_{15}d_{18}d_{21})W_1W_2}{d_{24}}, \\
&C_2 = a_{13}W_2 - a_{14}W_1^2, \ C_3 = b_{21}W_1W_2, \\
&C_4 = -\frac{d_{27}W_1 + (d_{15}d_{16}d_{21} + d_{15}d_{17}d_{22})W_1W_2}{d_{24}}, \\
&C_5 = b_{22}W_1W_2, \ C_6 = a_{11}W_1^2
\end{aligned} \tag{30}
$$

Next, by substituting Eqs. (28)-(29) into Eqs. (20)-(22) and applying the Galerkin method, we derive a system of equations to investigate the mechanical behavior of buckling and postbuckling in sandwich composite TSSs with an arch-type auxetic core and CNTRC face sheets, represented as:

$$
q - K_1\left(W_0 + \frac{W_2}{2}\right) - \frac{h}{R}\sigma_{0y} = 0 \tag{31}
$$

$$
l_{11} + l_{12}W_1^2 + l_{13}W_2 + l_{14}W_2^2 + hL^2n^2\sigma_{0y} = 0 \tag{32}
$$

$$
K_1W_0 + l_{16}W_1^2 + l_{17}W_2 + l_{18}W_1^2W_2 + \frac{h}{R}\sigma_{0y} = P_0 \tag{33}
$$

where the coefficients l_{ij} are obtained as explained by Dung and Vuong (2017).

Additionally, the TSSs must satisfy the circumferentially closed condition as

$$
\int_0^{2\pi R}\int_0^L v_{,y}\,dxdy = \int_0^{2\pi R}\int_0^L\left(\epsilon_y^0 + \frac{w}{R} - \frac{1}{2}w_{,y}^2\right)dxdy = 0 \tag{34}
$$

Table 1 Comparisons of critical buckling load $\bar{p}_{cr} = p_{cr}2\pi Rh$ (in KN) of CNTRC cylindrical shells subjected to radial pressure *(T = 300 K, R/h* = 100, *h* = 1 mm, $h_2 = 0$)

L^2/Rh	V_{CNT}	Shen *et al*. (2011b)		Present	
		UD	FG-X	UD	FG-X
100	0.12	18.75 (1,7)*	21.81 (1;7)	18.8321 (1,7)	21.638 (1,7)
	0.17	30.43 (1,7)	35.53 (1;7)	30.5419 (1,7)	35.2354 (1,7)
	0.28	37.77 (1,7)	47.18 (1;7)	38.0149 (1,7)	47.2022
300	0.12	19.35 (2,7)	22.06 (1,6)	19.4845 (2,7)	21.9109 (1,6)
	0.17	31.11 (2,7)	37.06 (1,6)	31.2862 (2,7)	36.8317
	0.28	39.60 (2,7)	46.52 (1,6)	39.9881 (2,7)	46.6537

*The numbers in brackets indicate the buckling modes (*m*, *n*)

Table 2 Comparison of critical buckling loads between CST and TSDT for convex TSSs with arc-type auxetic core and CNTRC face sheets, subjected to uniform external pressure and surrounded by a Kerr-type elastic foundation, across various R/h ratios. $(a = 4R, L = 1.5R, h_1 = 0.001mm, \bar{V}_{CNT} = 0.17, K_1 = K_2 = 0)$

convex	TSDT		CST		Difference (%)	
R/h	UD	FG-X	UD	FG-X	UD	FG-X
10	140.538 (1,3)	158.686 (1,3)	144.942 (1,3)	164.315 (1,3)	3.13	3.55
20	33.6545 (1,4)	36.0835 (1,3)	33.8147 (1,3)	36.2668 (1,3)	0.48	0.51
50	4.9076 (1,5)	5.33432 (1,5)	4.92158 (1,5)	5.35182 (1,5)	0.28	0.33
100	1.26582 (1,7)	1.3706 (1,7)	1.26758 (1,7)	1.37281 (1,7)	0.14	0.16
200	0.307379 (2,10)	0.334214 (2,10)	0.307599 (2,10)	0.334489 (2,10)	0.07	0.08

Using Eq. (18), Eq. (27), Eq. (28), and Eq. (29), this integral leads to

$$\frac{(2W_0 + W_2)}{R} - \left(\frac{n}{2R}\right)^2 W_1^2 - 2hI_2\sigma_{0y} = 0 \tag{35}$$

Inserting the average circumferential stress σ_{0y} from Eq. (31) into Eqs. (32)-(33), along with the circumferential closure condition of the shell, allows Eqs. (31)-(33) to be rewritten as

$$W_0 = S_{17}W_1^2 - W_2/2 + S_{18}P_0 \tag{36}$$

$$\begin{aligned} &S_{11} + S_{12}W_0 - S_{13}W_1^2 + l_{14}W_2 \\ &-S_{15}W_2^2 - S_{16}p_0 = 0 \end{aligned} \tag{37}$$

$$W_1^2 = \frac{S_{22}W_2}{S_{21} - S_{23}W_2} \tag{38}$$

Here, the expressions for S_{ij} are derived as outlined by Dung and Vuong (2017).

$$\left\{\begin{array}{c} \dfrac{S_{11}S_{22}}{-S_{22} + S_{23}W_2} \\ -S_{13}S_{21} - S_{12}S_{17}S_{21} + S_{14}S_{22} \\ +\dfrac{+S_{12}S_{18}S_{22} - S_{11}S_{23}}{-S_{22} + S_{23}W_2}W_2 \\ +\dfrac{-S_{15}S_{22} - S_{14}S_{23} - S_{12}S_{18}S_{23}}{-S_{22} + S_{23}W_2}W_2^2 \\ +\dfrac{S_{15}S_{23}}{-S_{22} + S_{23}W_2}W_2^3 \end{array}\right\} \times \left(\frac{1}{(S_{16} - S_{12}S_{19})}\right) \tag{39}$$

By setting $W_2 = 0$ in Eq. (39), the linear upper buckling load of the auxetic-core sandwich TSSs can be obtained as

$$p_0^{\text{upper}} = \frac{-S_{11}}{S_{16} - S_{12}S_{19}} \tag{40}$$

The critical buckling load for external pressure p_0^{cr} is determined by minimizing p_0^{upper} from Eq. (40) concerning *m* and *n*. From Eq. (27), the maximum deflection of the shells is given by

$$W_{\max} = W_0 + W_1 + W_2 \tag{41}$$

Inserting Eq. (36) and Eq. (38) into Eq. (41) yields the maximum deflection with respect to W_2.

$$W_{\max} = S_{17}W_1^2 + W_2/2 + S_{18}P_0 + \left(\frac{S_{22}W_2}{S_{21} - S_{23}W_2}\right)^{1/2} \tag{42}$$

Combining Eq. (39) and Eq. (42), one can obtain the postbuckling curve $P_0 - W_{max}/h$ of sandwich composite TSSs with an arch-type auxetic core and CNTRC face sheets.

5. Numerical results and discussion

5.1 Validation of the present study

As part of validating the current approach, comparative studies were conducted using the critical buckling loads derived by Shen *et al*. (2011b), who applied HSDT to a CNTRC cylindrical shell (assuming an infinite longitudinal radius) under external pressure. Table 1 shows that the validation cases demonstrate acceptable agreement between the two studies.

5.2 Importance of TSDT in evaluating buckling loads of thicker TSSs

In this section, to highlight the importance of TSDT, a comparative study is conducted on the critical buckling loads of auxetic core sandwich composite TSSs with CNTRC face sheets, subjected to uniform external pressure and supported by a Kerr-type elastic foundation, using both CST and TSDT approaches. The geometric parameters of the auxetic structure are specified as follows: $\theta = 60°$, $r_c = 2mm$, $d_1 = 2mm$, $E_c = 69GPa$. The analysis considers various *R/h* ratios and includes both convex (Table 2) and concave (Table 3) TSSs with two CNT distribution types: UD and FG-X. As observed, the discrepancy in the critical

Table 3 Comparison of critical buckling loads between CST and TSDT for convex TSSs with arc-type auxetic core and CNTRC face sheets, subjected to uniform external pressure and surrounded by a Kerr-type elastic foundation, across various R/h ratios. ($a = -4R$, $L = 1.5R$, $h_1 = 0.001mm$, $\bar{V}_{CNT} = 0.17$, $K_1 = K_2 = 0$)

convex	TSDT		CST		Difference (%)	
R/h	UD	FG-X	UD	FG-X	UD	FG-X
8	162.164 (1,3)	178.743 (1,2)	163.945 (1,2)	181.14 (1,2)	1.10	1.34
20	14.9114 (1,3)	17.2868 (1,3)	15.0545 (1,3)	17.4702 (1,3)	0.96	1.06
50	1.5553 (1,4)	1.827 (1,4)	1.5607 (1,4)	1.83381 (1,4)	0.35	0.37
100	0.198078 (1,4)	0.232178 (1,4)	0.198247 (1,4)	0.232392 (1,4)	0.09	0.09
200	0.02635530 (1,4)	0.03062490 (1,4)	0.02636060 (1,4)	0.0306316 (1,4)	0.02	0.02

Table 4 Comparison of critical buckling loads for sandwich composite TSSs with conventional versus re-entrant arc-type auxetic cores, featuring CNTRC face sheets under uniform external pressure at various ρ^*/ρ^s ratios ($R = 80h$, $\theta = 45°$, $L = 1.5R$, $h_1 = 0.001mm$, $\bar{V}_{CNT} = 0.17$, $K_1 = K_2 = 0$)

	Convex TSS ($a = 4R$)	Concave TSS($a = 4R$)
Re-entrant auxetic unit cell (Ebrahimi *et al*. 2024)		
$\rho^*/\rho^s = 0.1$ ($\gamma_1 = 2$, $\gamma_2 = 0.046$)	0.550893 (1,4)	0.241853 (1,3)
$\rho^*/\rho^s = 0.2$ ($\gamma_1 = 2$, $\gamma_2 = 0.091$)	0.553895 (1,4)	0.242679 (1,3)
$\rho^*/\rho^s = 0.3$ ($\gamma_1 = 2$, $\gamma_2 = 0.137$)	0.556767 (1,4)	0.243455 (1,3)
Arc-type auxetic unit cell		
$\rho^*/\rho^s = 0.1$ ($r_c = 5.73$, $d_1 = 1mm$)	0.554848 (1,4)	0.242459 (1,3)
$\rho^*/\rho^s = 0.2$ ($r_c = 5.01$`, $d_1 = 2mm$)	0.613509 (1,4)	0.25416 (1,3)
$\rho^*/\rho^s = 0.3$ ($r_c = 4.278\,mm$, $d_1 = 3mm$)	0.724365 (1,4)	0.274234 (1,3)

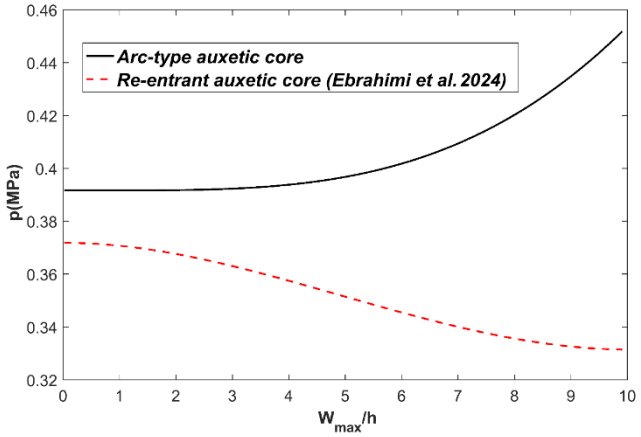

Fig. 3 Comparison of postbuckling curves for sandwich composite TSSs with conventional versus re-entrant arc-type auxetic cores (L = 1.5R, R/h = 80, a = -4R, θ = 45°, γ_1 = 2, γ_2 = 0.137, r_c = 4.278 mm, d_1 = 3 mm, *UD - CNT*, *y* - direction, V_{CNT} = 0.28, $k_1 = k_2 = 0$)

buckling loads between CST and TSDT is minimal for thin shells. However, for thicker shells, this difference becomes more pronounced. For instance, for convex TSSs (Table 2), at $R/h = 200$ (thin shell) with the FG-X CNT distribution, the critical load p_0^{cr} is 0.334489 MPa (CST) compared to 0.334214 MPa (TSDT), yielding a discrepancy of 0.08%. In contrast, at $R/h = 10$ (thick shell), the discrepancy increases to 3.55%. Similarly, for concave TSSs, the difference is 0.02% at $R/h = 200$, rising to 1.34% at $R/h = 8$. The table further shows that the discrepancy is higher for the FG-X distribution compared to UD, as expected, and is more significant for concave shells than for convex shells.

5.3 Effects of an arc-type auxetic core

Table 4 presents a comparative study of the buckling characteristics of sandwich-structured TSSs with two auxetic core designs: a conventional re-entrant auxetic structure, as analyzed by Ebrahimi *et al*. (2024), and an arc-type auxetic structure. The analysis considers different geometric parameters of the unit cells while maintaining a constant relative density, ρ^*/ρ^s (Ashby and Gibson 1997), in which ρ^* and ρ^s denote the density of unit cell and solid material, respectively. The results indicate that the arc-type auxetic structure consistently outperforms the conventional re-entrant structure in buckling performance, with this advantage becoming more significant at higher relative densities. For instance, at $\rho^*/\rho^s = 0.3$, the buckling load of the arc-type structure shows a 30.10% increase for convex TSSs and a 12.64% increase for concave TSSs.

Fig. 3 highlights the advantages of the arc-type auxetic core over the conventional re-entrant core, both having the same relative density in the postbuckling behavior of convex TSSs. The curves show that the arc-type core achieves higher loads and greater strength. Additionally, snap-through behavior is observed in the re-entrant core but is absent in the arc-type core.

Next, we examine the effects of the geometric parameters of an arc-type auxetic core on the buckling and postbuckling performance of sandwich TSSs with CNT-reinforced face sheets. Tables 5and 6 present the critical buckling loads for both convex and concave sandwich TSSs, evaluated for various arc radii (r_c = 2 mm, 4 mm, 6 mm, and 8 mm) and inclined angles ($\theta = 8°$, $\theta = 12°$, $\theta = 20°$, and $\theta = 45°$). The results indicate that increasing the unit cell's arc radius (r_c) decreases the critical buckling load for both convex and concave TSSs. Specifically, convex TSSs with an arc radius of 8 mm (with $\theta = 8°$) exhibit an 88.05% reduction in critical buckling load compared to those with an arc radius of 2 mm. Similarly, concave TSSs with the same auxetic core geometry show an 86.09% decrease in critical buckling load.

Regarding the influence of the inclination angle, a decrease in θ results in a higher buckling load. For instance, convex TSSs at $\theta = 8°$ (with r_c = 2 mm) show a 650.51% improvement in buckling load compared to those with $\theta = 45°$. Similarly, for concave TSSs, a 1089.65% increase in buckling load is observed under the same unit cell geometric parameters.

Table 5 Influence of arc radius and inclined angle on the critical buckling loads of convex sandwich TSSs ($a = 4R, L = 1.5R, h_1 = 0.001mm, \bar{V}_{CNT} = 0.17, K_l = K_u = 10^7,\ K_s = 10^5$)

Inclined angle θ	$r_c = 2\ mm$	$r_c = 4\ mm$	$r_c = 6mm$	$r_c = 8\ mm$
$\theta = 8°$	16.6313 (1,2)	4.7186 (2,4)	2.5237 (2,4)	1.9868 (2,4)
$\theta = 12°$	7.7587(2,4)	2.3675 (2,4)	1.8200 (2,4)	1.6819 (2,4)
$\theta = 20°$	3.4816 (3,6)	1.7612 (3,6)	1.4561 (2,5)	1.2484 (1,4)
$\theta = 45°$	2.2160 (2,6)	1.2010 (1,5)	1.0567 (1,5)	0.9909 (1,5)

Table 6 Influence of arc radius and inclined angle on the critical buckling loads of concave sandwich TSSs ($a = -4R, L = 1.5R, h_1 = 0.001mm, \bar{V}_{CNT} = 0.17, K_l = K_u = 10^7, K_s = 10^5$)

Inclined angle θ	$r_c = 2\ mm$	$r_c = 4\ mm$	$r_c = 6mm$	$r_c = 8\ mm$
$\theta = 8°$	10.6069 (1,2)	3.1800 (1,2)	1.9887 (2,4)	1.4753 (2,4)
$\theta = 12°$	5.8997 (1,2)	1.7444 (2,4)	1.2900 (2,4)	1.1072 (1,3)
$\theta = 20°$	2.3138 (2,4)	1.1243 (1,3)	0.8208 (1,3)	0.7465 (1,3)
$\theta = 45°$	0.8916 (1,4)	0.6554 (1,4)	0.6292 (1,4)	0.6194 (1,4)

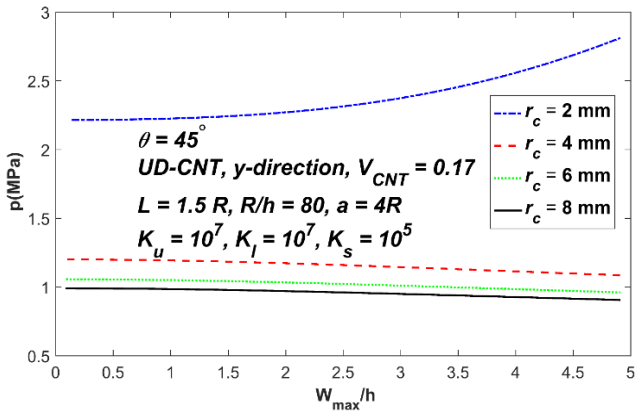

Fig. 4 Effect of arc radius on the postbuckling curves of convex auxetic-core sandwich TSSs

The impacts of the auxetic core's geometric parameters on the postbuckling characteristics of convex and concave sandwich composite TSSs are presented in Figs. 4-7. Fig. 4 and 5 show that reducing the arc radius significantly enhances both TSS types' postbuckling strength and load-bearing capacity. In convex TSSs, larger arc radius values trigger snap-through behavior, indicating a sudden change in structural response. Additionally, the onset of snap-through behavior is clearly observed in convex TSSs for larger values of r_c, which signifies a sudden transition in the shell's structural response.

Subsequently, Figs. 6-7 illustrate the influence of the inclined angle on postbuckling curves. Lower θ values yield higher postbuckling curves, improving stability. For instance, at $\theta = 8°$, maximum postbuckling strength is attained, while at $\theta = 45°$, the curves exhibit a flattening trend, indicating decreased stiffness and stability under additional loading.

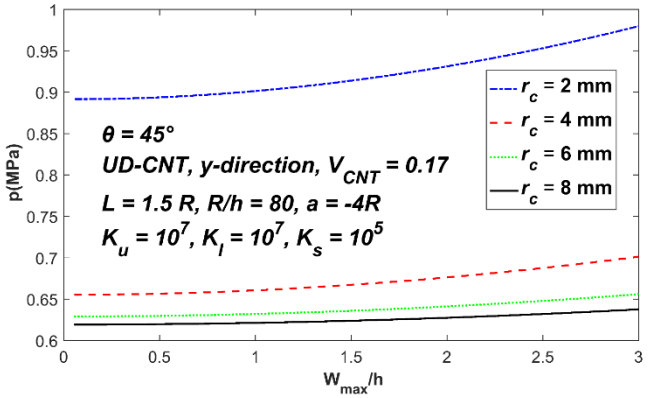

Fig. 5 Effect of arc radius on the postbuckling curves of concave auxetic-core sandwich TSSs

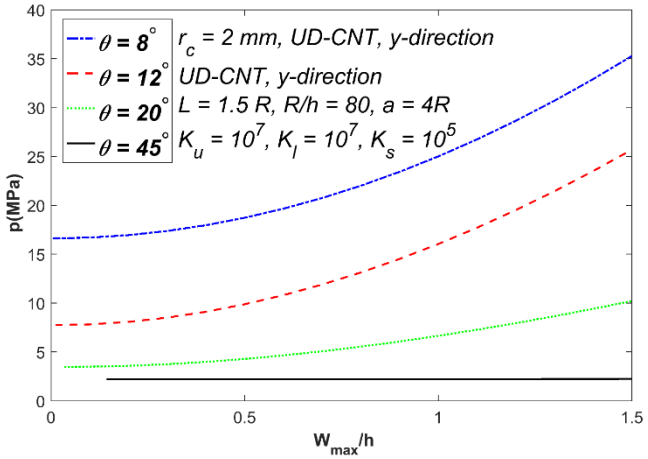

Fig. 6 Effect of inclined angle on the postbuckling curves of convex auxetic-core sandwich TSSs

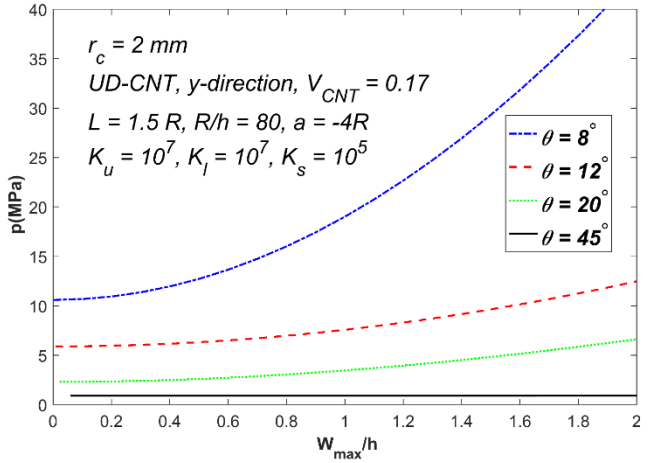

Fig. 7 Influence of inclined angle on the postbuckling curves of concave auxetic-core sandwich TSSs

5.4 Effects of Kerr-type elastic foundation

In what continues, the effect of the Kerr-type foundation on the buckling and postbuckling performance of sandwich composite TSSs is investigated.

As the first case, Figs. 8 and 9 illustrate the postbuckling

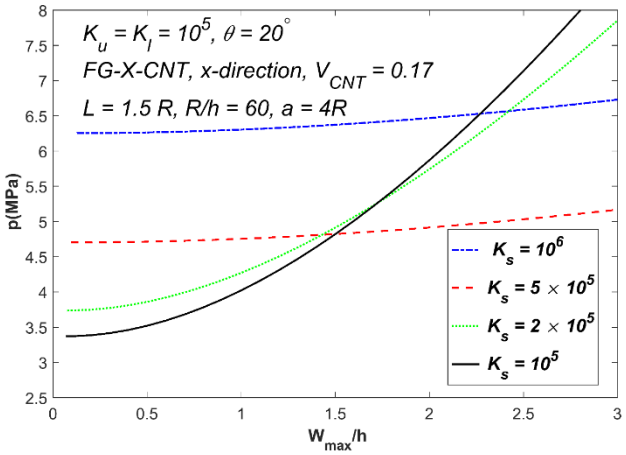

Fig. 8 Influence of the Kerr foundation's shear layer on the postbuckling curves of convex TSSs

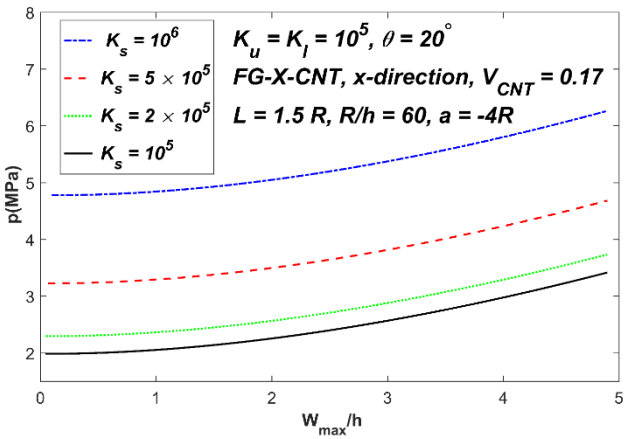

Fig. 9 Influence of the Kerr foundation's shear layer on the postbuckling curves of concave TSSs

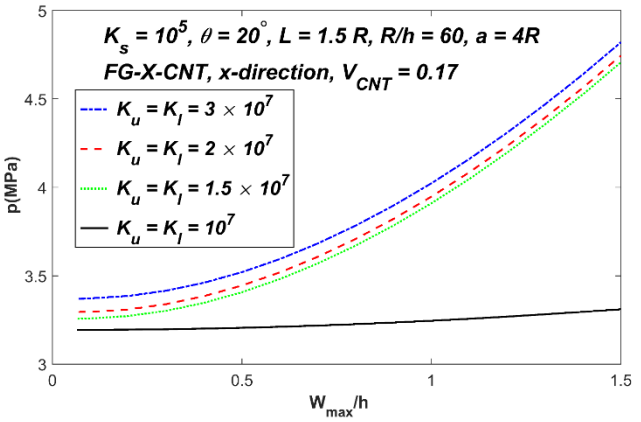

Fig. 10 Influence of the Kerr foundation's linear layer on the postbuckling curves of convex TSSs

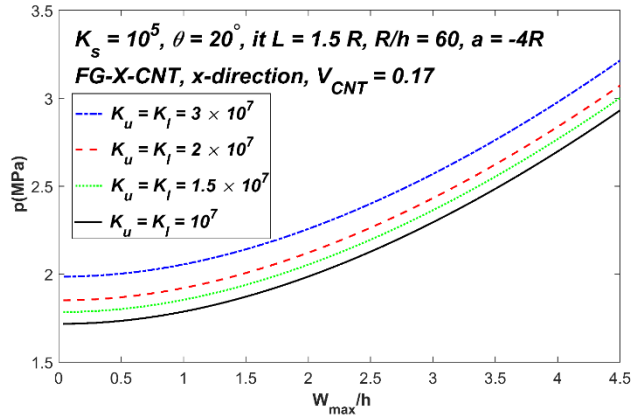

Fig. 11 Influence of the Kerr foundation's linear layer on the postbuckling curves of concave TSSs

behavior of convex and concave TSSs for varying shear layer stiffness K_s values. Both figures show that as K_s increases, the postbuckling curves show a significant rise in load-bearing capacity at a given displacement $W_{\max}/h$. This trend emphasizes the stabilizing effect of a stiffer sheer foundation, enhancing structural resistance to postbuckling deformations. For the convex shell (Fig. 8), lower K_s values result in steeper postbuckling curves, especially at the initial displacement stages. As K_s increases, the curves become less steep, reflecting a more gradual and stable post-buckling response. The load-bearing capacity progressively increases with $W_{\max}/h$, indicating that a stiffer foundation reduces the likelihood of abrupt changes in load-bearing behavior, thereby enhancing the shell's resilience in the postbuckling regime. In the concave shell, the postbuckling load-displacement curves consistently show a similar upward trend, with initial load-displacement responses that are less steep, even at lower K_s values (Fig. 9). This suggests a more gradual increase in load-bearing capacity compared to the convex shell. A key observation for both shells is that as the foundation stiffness K_s increases, the likelihood of snap-through behavior decreases significantly.

The influence of the Kerr-type foundation parameters K_l and K_u on the postbuckling behavior of both convex and concave TSSs is illustrated in Figs. 10 and 11. Increasing the stiffness of the Kerr substrate's linear layers leads to a higher critical buckling load and more elevated postbuckling curves, reflecting the stability-enhancing effect also seen with increased shear layer stiffness. This indicates that a stiffer Kerr foundation significantly improves structural stability, resulting in steady, upward-sloping postbuckling curves and eliminating any signs of snap-through behavior.

6. Conclusions

This paper provides analytical solutions for the nonlinear buckling and postbuckling behavior of shear-deformable, arc-type auxetic-core sandwich TSSs with CNT-reinforced face sheets surrounded by a Kerr-type foundation and subjected to external pressure. Fundamental equations are derived using the Airy stress function and TSDT, incorporating von Kármán-type geometric nonlinearity, with the Galerkin procedure employed to determine explicit load-deflection relationships. The numerical findings yield several key insights:

• For thin TSSs, the difference between critical buckling loads obtained from CST and TSDT is minimal, validating

the applicability of CST for these cases. Therefore, CST is sufficient to study the stability of thin shells. However, for thicker shells, where discrepancies up to 3.55% are observed—particularly with FG-X CNT distribution and concave shapes—TSDT provides a more accurate stability analysis, demonstrating its necessity for thicker TSSs.

• The arc-type auxetic core demonstrates superior buckling and postbuckling performance over the conventional re-entrant core, particularly at higher relative density.

• Increasing the auxetic core's unit cells r_c leads to a reduction in critical buckling loads for both shell types, with convex TSSs showing up to an 88.05% decrease and concave TSSs an 86.09% decrease when comparing $r_c = 8$ mm to $r_c = 2$ mm. Similarly, decreasing unit cells' θ enhances stability, significantly raising the buckling load; for convex TSSs, lowering θ from 45° to 8° achieves a 650.51% increase in buckling load, while concave shells see a 1089.65% improvement under similar conditions. Additionally, in the postbuckling regime, smaller r_c values contribute to stronger and more stable load-bearing performance. In comparison, larger r_c values trigger snap-through behavior, highlighting a transition in structural response for convex shells. Lower θ values similarly yield higher postbuckling curves, indicating improved stability and resistance to deformation under continued loading. This highlights the significance of optimizing r_c and θ to enhance the buckling resilience and postbuckling strength of auxetic-core TSSs.

• Increased stiffness in both the shear and linear foundation layers significantly enhances the shells' load-bearing capacity in the postbuckling regime and reduces snap-through behavior. This higher stiffness raises the critical buckling load and improves stability, resulting in smoother, upward-sloping postbuckling curves for both convex and concave shells.

References

Ashby, M.F. and Gibson, L.J. (1997), *Cellular Solids: Structure and Properties*, 175-231, Press Syndicate of the University of Cambridge, Cambridge, U.K. https://doi.org/10.1017/CBO9781139878326

Chakraborty, S. and Dey, T. (2023), "Thermomechanical buckling and wrinkling characteristics of softcore sandwich panels with CNT reinforced composite face sheets", *Eur. J. Mech. A Solids*, **98**, 104894. https://doi.org/10.1016/j.euromechsol.2022.104894

Ebrahimi, F. (2024), *Mechanics of Auxetic Materials and Structures*, CRC Press.

Ebrahimi, F., Goudarzfallahi, M. and Ziazi, A.A. (2024a), "Static stability analysis of graphene origami-reinforced nanocomposite toroidal shells with various auxetic cores", *Adv. Nano Res.*, **17**(1), 1. https://doi.org/10.12989/anr.2024.17.1.001

Ebrahimi, F., Goudarzfallahi, M. and Ziazi, A.A. (2024b), "Porosity effects on the buckling and post buckling of metamaterial sandwich toroidal shell segments", *Steel Compos. Struct.*, **53**(3), 313-326. https://doi.org/10.12989/scs.2024.53.3.313

Ebrahimi, F. and Dabbagh, A. (2023), "Porosity effects on static performance of carbon nanotube-reinforced meta-nanocomposite structures", *Micromachines*, **14**(7), 1402. https://doi.org/10.3390/mi14071402

Ebrahimi, F. and Dadashi, M. (2023), "Composite cylindrical shells with auxetic core on elastic foundation: A nonlinear dynamic analysis", *Structures*, **57**, 105170. https://doi.org/10.1016/j.istruc.2023.105170

Duc, N.D., Kim, S.E., Quan, T.Q., Manh, D.T. and Cuong, N.H. (2020), "Nonlinear buckling of eccentrically stiffened nano-composite cylindrical panels in thermal environments", *Thin Wall. Struct.*, **146**, 106428. https://doi.org/10.1016/j.tws.2019.106428

Dung, D.V. and Vuong, P.M. (2017), "Analytical investigation on buckling and postbuckling of FGM toroidal shell segment surrounded by elastic foundation in thermal environment and under external pressure using TSDT", *Acta Mechanica*, **228**(10), 3511-3531. https://doi.org/10.1007/s00707-017-1888-2

Ebrahimi, F. and Ahari, M.F. (2024), "On the buckling of meta-graphene-origami-enabled magnetostrictive nanoplates under temperature gradient", *Acta*, **235**, 2611-2628. https://doi.org/10.1007/s00707-024-03861-x

Ebrahimi, F. and Dabbagh, A. (2020), *Mechanics of Nanocomposites: Homogenization and Analysis*, CRC Press.

Fu, T., Wang, X., Hu, X. and Rabczuk, T. (2024), "Impact dynamic response of stiffened porous functionally graded materials sandwich doubly-curved shells with Arc-type auxetic core", *Int. J. Impact Eng.*, **191**, 105000. https://doi.org/10.1016/j.ijimpeng.2024.105000

Ebrahimi, F. and Seyfi, A. (2022), "Studying propagation of wave of metal foam rectangular plates with graded porosities resting on Kerr substrate in thermal environment via analytical method", *Waves Random Complex Med.*, **32**(2), 832-855. https://doi.org/10.1080/17455030.2020.1802531

Fu, T., Wang, X., Hu, X. and Rabczuk, T. (2024), "Impact dynamic response of stiffened porous functionally graded materials sandwich doubly-curved shells with Arc-type auxetic core", *Int. J. Impact Eng.*, **191**, 105000. https://doi.org/10.1016/j.ijimpeng.2024.105000

Ghafouri, M., Ghassabi, M. and Talebitooti, R. (2023), "Applying a 3D re-entrant auxetic cellular core to a graphene nanoplatelet–reinforced doubly curved structure: A sound transmission loss study", *J. Eng. Mech.*, **149**(10), 04023077. https://doi.org/10.1061/JENMDT.EMENG-6978

Hieu, P.T. and Van Tung, H. (2021), "Thermal buckling and postbuckling of CNT-reinforced composite cylindrical shell surrounded by an elastic medium with tangentially restrained edges", *J. Thermoplast. Compos. Mater.*, **34**(7), 861-883. https://doi.org/10.1177/0892705719853611

Hieu, P.T. and Van Tung, H. (2020a), "Buckling of shear deformable FG-CNTRC cylindrical shells and toroidal shell segments under mechanical loads in thermal environments", *ZAMM J. Appl. Math. Mech.*, **100**(11), e201900243. https://doi.org/10.1177/0892705719853611

Hieu, P.T. and Van Tung, H. (2020b), "Thermal and thermo-mechanical buckling of shear deformable FG-CNTRC cylindrical shells and toroidal shell segments with tangentially restrained edges", *Arch. Appl. Mech.*, **90**(7), 1529-1546. https://doi.org/10.1007/s00419-020-01682-7

Hoai Nam, V., Ngoc Ly, L., Thi Kieu My, D., Minh Duc, V. and Thi Phuong, N. (2024), "On the nonlinear buckling and postbuckling responses of sandwich FG-GRC toroidal shell segments with corrugated core under axial tension and compression in the thermal environment", *Polym. Compos.*, **45**(15), 13737-13752. https://doi.org/10.1002/pc.28732

Hutchinson, J.W. (1967), "Initial post-buckling behavior of toroidal shell segments", *Int. J. Solids Struct.*, **3**(1), 97-115. https://doi.org/10.1016/0020-7683(67)90046-7

Li, Y.S. and Liu, B.L. (2022), "Thermal buckling and free vibration of viscoelastic functionally graded sandwich shells with tunable auxetic honeycomb core", *Appl. Math. Modell.*, **108**, 685-700. https://doi.org/10.1016/j.apm.2022.04.019

Li, C., Shen, H.S. and Wang, H. (2020a), "Nonlinear dynamic response of sandwich plates with functionally graded auxetic 3D lattice core", *Nonlinear Dyn*., **100**, 3235-3252. https://doi.org/10.1007/s11071-020-05686-4

Li, C., Shen, H.S. and Wang, H. (2020b), "Nonlinear dynamic response of sandwich plates with functionally graded auxetic 3D lattice core", *Nonlinear Dyn*., **100**, 3235-3252. https://doi.org/10.1007/s11071-020-05686-4

Mahinzare, M., Rastgoo, A. and Ebrahimi, F. (2024), "On nonlinear vibration of piezo-electrically multiscale hybrid nanocomposite sandwich plate including an auxetic core based on HSDT", *Int. J. Struct. Stabil. Dyn*., **24**(5). https://doi.org/10.1142/S021945542450069X

Nam, V.H., Duc, V.M., Doan, C.V., Thanh Xuan, N.T. and Phuong, N.T. (2022), "Nonlinear postbuckling behavior of auxetic-core toroidal shell segments with Graphene reinforced face sheets under axial loads", *Arch. Mech*., **74**(2-3). http://doi.org/10.24423/aom.3957

Nguyen, T.P., Vu, M.D., Dang, T.D., Cao, V.D., Pham, T.H. and Vu, H.N. (2023), "An analytical approach of nonlinear buckling behavior of torsionally loaded auxetic core toroidal shell segments with graphene reinforced polymer coatings", *Adv. Compos. Mater*., **32**(3), 400-418. https://doi.org/10.1080/09243046.2022.2110661

Oyesanya, M.O. (2005), "Influence of extra terms on asymptotic analysis of imperfection sensitivity of toroidal shell segment with random imperfection", *Mech. Res. Commun*., **32**(4), 444-453. https://doi.org/10.1016/j.mechrescom.2005.02.006

Phuong, N.T., Van Doan, C., Duc, V.M., Giang, N.T. and Nam, V.H. (2023), "Analytical solution for nonlinear buckling of convex and concave auxetic-core toroidal shell segments with graphene-reinforced face sheets subjected to radial loads", *Arch. Appl. Mech*., **93**(2), 621-634. https://doi.org/10.1007/s00419-022-02288-x

Phuong, N.T., Nam, V.H., Trung, N.T., Duc, V.M., Van Loi, N., Thinh, N.D. and Tu, P.T. (2021), "Thermomechanical post-buckling of functionally graded graphene-reinforced composite laminated toroidal shell segments surrounded by Pasternak's elastic foundation", *J. Thermoplast. Compos. Mater*., **34**(10), 1380-1407. https://doi.org/10.1177/0892705719870593

Reddy, J.N. and Liu, C.F. (1987), *A Higher-Order Theory for Geometrically Nonlinear Analysis of Composite Laminates*, No. VPI-E-86.21, NASA.

Reddy, J.N. (2003), *Mechanics of laminated composite plates and shells: Theory and analysis*, CRC press.

Shen, H.S. (2011a), "Postbuckling of nanotube-reinforced composite cylindrical shells in thermal environments, Part I: Axially-loaded shells", *Compos. Struct*., **93**(8), 2096-2108. https://doi.org/10.1016/j.compstruct.2011.02.011

Shen, H.S. (2011b), "Postbuckling of nanotube-reinforced composite cylindrical shells in thermal environments, Part II: Pressure-loaded shells", *Compos. Struct*., **93**(10), 2496-2503. https://doi.org/10.1016/j.compstruct.2011.04.005

Shen, H.S. and Xiang, Y. (2013), "Postbuckling of nanotube-reinforced composite cylindrical shells under combined axial and radial mechanical loads in thermal environment", *Compos. Part B Eng*., **52**, 311-322. https://doi.org/10.1016/j.compositesb.2013.04.034

Sofiyev, A.H. and Kuruoglu, N.U.R.İ. (2022), "Buckling analysis of shear deformable composite conical shells reinforced by CNTs subjected to combined loading on the two-parameter elastic foundation", *Defence Technol*., **18**(2), 205-218. https://doi.org/10.1016/j.dt.2020.12.007

Stein, M. and McElman, J.A. (1965), "Buckling of segments of toroidal shells", *AIAA J*., **3**(9), 1704-1709. https://doi.org/10.2514/3.55185

Van Quyen, N., Van Thanh, N., Quan, T.Q. and Duc, N.D. (2021), "Nonlinear forced vibration of sandwich cylindrical panel with negative Poisson's ratio auxetic honeycombs core and CNTRC face sheets", *Thin Wall. Struct*., **162**, 107571. https://doi.org/10.1016/j.tws.2021.107571

Van Tien, N., Duc, V.M., Nam, V.H., Phuong, N.T., Ho, L.S., Dong, D.T., Ly, L.N., Hung, D. and Minh, T.Q. (2022), "Nonlinear postbuckling of auxetic-core sandwich toroidal shell segments with CNT-reinforced face sheets under external pressure", *Int. J. Struct. Stabil. Dyn*., **22**(1), 2250006. https://doi.org/10.1142/S0219455422500067

Vuong, P.M. and Duc, N.D. (2019), "Nonlinear buckling and postbuckling of a FGM toroidal shell segment under a torsional load in a thermal environment within Reddy's third-order shear deformation shell theory", *Mech. Compos. Mater*., **55**, 467-482. https://doi.org/10.1007/s11029-019-09826-9

Vuong, P.M. and Duc, N.D. (2020a), "Nonlinear static and dynamic stability of functionally graded toroidal shell segments under axial compression", *Thin Wall. Struct*., **155**, 106973. https://doi.org/10.1016/j.tws.2020.106973

Vuong, P. M. and Duc, N.D. (2020b), "Nonlinear buckling and post-buckling behavior of shear deformable sandwich toroidal shell segments with functionally graded core subjected to axial compression and thermal loads", *Aerosp. Sci. Technol*., **106**, 106084. https://doi.org/10.1016/j.ast.2020.106084

Wang, X. and Fu, T. (2024), "A novel arc-type auxetic cellular doubly-curved shells with negative Poisson's ratio for broadband low-frequency sound insulation", *Eur. J. Mech. A Solids*, **106**, 105326. https://doi.org/10.1016/j.euromechsol.2024.105326

Zhao, L.C., Xu, L. and Zeng, H.T. (2024), "Thermal buckling of temperature-dependent FG-CNT reinforced composite conical-conical joined shell using GDQ", *Thin Wall. Struct*., **205**, 112320. https://doi.org/10.1016/j.tws.2024.112320

CC